Computer Assisted Methods in Engineering and Science, **22**: 289–300, 2015.

Method of regularized sources for two-dimensional Stokes flow problems based on rational or exponential blobs

Shiting Wen[1], Kai Wang[1], Rizwan Zahoor[2],
Ming Li[1], Bozidar Šarler[1,2,3]

[1] *College of Mathematics*
Taiyuan University of Technology
Yingze West Street 79, 030024 Taiyuan, Shanxi Province, China

[2] *Laboratory for Multiphase Processes*
University of Nova Gorica
Vipavska 13, SI-5000, Nova Gorica, Slovenia

[3] *Laboratory for Simulation of Materials and Processes*
Institute of Metals and Technology
Lepi pot 11, SI-1000, Ljubljana, Slovenia
e-mail: bozidar.sarler@ung.si

The solution of Stokes flow problems with Dirichlet and Neumann boundary conditions is performed by a non-singular method of fundamental solutions (MFS) which does not require artificial boundary, i.e., source points of fundamental solution coincide with the collocation points on the boundary. The fundamental solution of the Stokes pressure and velocity is obtained from the analytical solution due to the action of the Dirac delta- type force. Instead of Dirac delta force, a non-singular function called blob, with a free parameter epsilon is employed, which is limited to Dirac delta function when epsilon is limited to zero. The analytical expressions for related Stokes flow pressure and velocity around such regularized sources have been derived for rational and exponential blobs in an ordered way. The solution of the problem is sought as a linear combination of the fields due to the regularized sources that coincide with the boundary and with their intensities chosen in such a way that the solution complies with the boundary conditions. A numerical example for two-dimensional (2D) driven cavity and a flow between parallel plates are chosen to assess the properties of the method. The results of the posed method of regularized sources (MRS have been compared with the results obtained by the fine-grid second-order classical finite difference method (FDM) and analytical solution. The results converge with finer discretisation; however, they depend on the value of epsilon. The method gives reasonably accurate results for the range of epsilon between 0.1 and 0.5 of the typical nodal distance on the boundary. Exponential blobs give slightly better results than the rational blobs; however, they require slightly more computing time. A robust and efficient strategy to find the optimal value of epsilon is needed in the perspective.

Keywords: Stokes flow, regularized sources, rational blobs, exponential blobs, meshless method, driven cavity problem, convergence study.

1. Introduction

Stokes or creeping flow is a type of fluid flow [1] where the inertial forces are small compared with the viscous forces. This typically occurs in situations where the fluid velocities are very slow, the viscosities are very large, or the length-scales of the flow are very small. Stokes flow occurs in many natural and technological systems. In nature, for example, this type of flow occurs in swimming of microorganisms as well as in the flow of lava. In technology, for example, Stokes flow is important in the mushy zone of metal solidification in castings and in the flow of viscous polymers. Consequently, Stokes flow appears also in a spectrum of biomedical situations such as the capillary blood flow

in the cardiovascular systems and the capillary air flow in the lungs. The present research was stimulated by the simulation needs in microfluidics [2].

The method of fundamental solutions (MFS) [3] has been widely applied in recent years to the computational analysis of fluid flows. The MFS belongs to the boundary meshless methods. The solution in MFS is represented by trial functions defined by fundamental solutions of the governing equation. Their expansion coefficients match, in collocation or least squares sense, the boundary conditions. Since the fundamental solution is usually singular, the source points are in general not allowed to be placed on the boundary. Their position forms the so-called artificial boundary. This represents the main disadvantage of the classical MFS, which is particularly pronounced in geometrically complex and multi-region situations. The first ideas regarding how to overcome the artificial boundary issue were presented by Young et al. [4], where the desingularization was performed through the properties of double layer potential. Since 2006, several publications appeared on the subject of non-singular MFS, treating the spectra of different partial differential equations. Young et al. [5] developed classical MFS for 2D and three-dimensional (3D) Stokes flows, based on the Stokes fundamental solution. Curteanu et al. [6] developed a classical MFS solution of Stokes flow by using Laplace decomposition and Laplace fundamental solution. The pioneering developments of the non-singular MFS for potential flow, Darcy flow and Stokes flow appear in [7–9], respectively. The desingularization was achieved by integration of the fundamental solution over a small vicinity of the singularity. In the case of Neumann boundary conditions, reference solutions need to be constructed for resolving the diagonal coefficients. Cortez desingularized the Stokes flow fundamental solution by introducing smoothed sources instead of delta sources, which appear in the classical fundamental solution, and, next, he applied this method to 2D [10] and 3D [11] flow problems. The authors of this paper have recently derived the method for axisymmetric Stokes flow problems [12]. Our approach was rederived for different types of boundary conditions as well as external and internal Stokes flow problems. In this paper, we conduct a systematic sensitivity study on the accuracy of the method as a function of the rational and exponential desingularization function types and desingularization parameter, using the example of a driven cavity problem and a flow between parallel plates.

2. Governing equations

Let us consider a fixed domain Ω with a boundary Γ filled with fluid that exhibits steady incompressible Stokes flow with constant fluid viscosity. The boundary value problem is governed by the following set of mass and momentum conservation equations:

$$\nabla \cdot \mathbf{v}(\mathbf{p}) = 0, \tag{1}$$

$$-\nabla P(\mathbf{p}) + \mu \nabla^2 \mathbf{v}(\mathbf{p}) + \mathbf{f}(\mathbf{p}) = 0, \tag{2}$$

boundary conditions of the Dirichlet type are

$$v_\varsigma(\mathbf{p}) = \overline{v}_\varsigma(\mathbf{p}); \quad \mathbf{p} \in \Gamma_\varsigma^D, \tag{3}$$

and the Neumann type are

$$\partial v_\varsigma(\mathbf{p}) / \partial p_\xi = \overline{v}_{\varsigma\xi}(\mathbf{p}); \quad \mathbf{p} \in \Gamma_{\xi\varsigma}^N, \tag{4}$$

where $\mathbf{p}$ represents position vector, $\mathbf{v}$ velocity, P pressure, μ viscosity, $\mathbf{f}$ the body force, Γ_ς^D Dirichlet part of the boundary for coordinate ς, $\Gamma_{\varsigma\xi}^N$ Neumann part of the boundary for the coordinate ς and derivative over coordinate ξ, respectively, and $\overline{v}_\varsigma$ and $\overline{v}_{\varsigma\xi}$ stand for known boundary conditions forcing functions. We seek the solution of the pressure and the velocity field in the Ω and unknown parts of Γ.

3. Solution procedure

The Stokes flow solution in point $\mathbf{p}$ around the source of the type $\mathbf{f}(\mathbf{p},\mathbf{s}) = \mathbf{f}_{\varepsilon}\phi(\mathbf{p}-\mathbf{s})$ is given in point $\mathbf{s}$ by

$$\mathbf{v}(\mathbf{p},\mathbf{s}) = \left[(\mathbf{f}\cdot\nabla)\nabla_{\varepsilon}\widehat{\widehat{\phi}}(\mathbf{p}-\mathbf{s}) - \mathbf{f}\,{}_{\varepsilon}\widehat{\phi}(\mathbf{p}-\mathbf{s})\right]\Big/\mu, \tag{5}$$

$$P(\mathbf{p},\mathbf{s}) = \mathbf{f}\cdot\nabla_{\varepsilon}\widehat{\phi}(\mathbf{p}-\mathbf{s}), \tag{6}$$

with

$$\nabla^2{}_{\varepsilon}\widehat{\phi} = {}_{\varepsilon}\phi, \tag{7}$$

$$\nabla^2{}_{\varepsilon}\widehat{\widehat{\phi}} = {}_{\varepsilon}\widehat{\phi}. \tag{8}$$

In the case when the Dirac delta function $\delta(\mathbf{p}-\mathbf{s})$ is selected for function ${}_{\varepsilon}\varphi(\mathbf{p}-\mathbf{s})$, Eqs. (5)–(8) give the well-known Stokes fundamental pressure and velocity. Let us Consider a 2D situation with $\mathbf{p} = p_x\mathbf{i}_x + p_y\mathbf{i}_y$ (p_ς and $\mathbf{i}_\varsigma$ stand for Cartesian coordinates and base vectors, respectively). The governing equations are thus as follows:

$$\frac{\partial v_x(p_x,p_y)}{\partial p_x} + \frac{\partial v_y(p_x,p_y)}{\partial p_y} = 0, \tag{9}$$

$$-\frac{\partial P(p_x,p_y)}{\partial p_x} + \mu\left(\frac{\partial^2 v_x(p_x,p_y)}{\partial p_x^2} + \frac{\partial^2 v_x(p_x,p_y)}{\partial p_y^2}\right) + f_x(s_x,s_y)\,{}_{\varepsilon}\phi(p_x,p_y,s_x,s_y) = 0, \tag{10}$$

$$-\frac{\partial P(p_x,p_y)}{\partial p_y} + \mu\left(\frac{\partial^2 v_y(p_x,p_y)}{\partial p_x^2} + \frac{\partial^2 v_y(p_x,p_y)}{\partial p_y^2}\right) + f_y(s_x,s_y)\,{}_{\varepsilon}\phi(p_x,p_y,s_x,s_y) = 0. \tag{11}$$

Instead of selecting the Dirac delta function for the source shape, two different non-singular functions called blobs [10] are introduced in this paper. The rational blob is

$$\begin{aligned} {}_{\varepsilon\,\mathrm{rat}}\phi(\mathbf{p}-\mathbf{s}) &= \frac{3\varepsilon^3}{2\pi}\left(|\mathbf{p}-\mathbf{s}|^2+\varepsilon^2\right)^{-5/2}, \\ |\mathbf{p}-\mathbf{s}|^2 &= r^2 = (p_x-s_x)^2 + (p_y-s_y)^2, \end{aligned} \tag{12}$$

and the exponential blob is

$${}_{\varepsilon\,\exp}\phi(\mathbf{p}-\mathbf{s}) = \frac{1}{\pi\varepsilon^2}\exp\left(-\frac{|\mathbf{p}-\mathbf{s}|^2}{\varepsilon^2}\right), \tag{13}$$

where ε stands for the shape parameter. These functions have the same strength as the Dirac delta function, $\int\limits_{\Omega}\delta d\Omega = 1$, i.e., $\int\limits_{0}^{\infty}{}_{\varepsilon}\phi(r(\mathbf{p}-\mathbf{s}))2\pi r dr = 1$; $r \in 2D$, and they approach the Dirac delta function when $\varepsilon \to 0$. The corresponding harmonic (7) and biharmonic equation (8) functions have been obtained through the following formulas:

$$\begin{aligned} \nabla^2_{\varepsilon}\widehat{\phi}(r) &= \frac{1}{r}\frac{\partial}{\partial r}\left[r\frac{\partial}{\partial r}{}_{\varepsilon}\widehat{\phi}(r)\right] = {}_{\varepsilon}\phi, \\ \frac{\partial}{\partial r}{}_{\varepsilon}\widehat{\phi} &= \frac{1}{r}\int r\,{}_{\varepsilon}\phi(r)dr + \frac{c_1}{r}, \\ {}_{\varepsilon}\widehat{\phi} &= \int\frac{1}{r}\left[\int r\,{}_{\varepsilon}\phi(r)dr\right]dr + c_1\log(r) + c_2, \end{aligned} \tag{14}$$

$$\nabla_\varepsilon^2 \widehat{\widehat{\phi}}(r) = \frac{1}{r}\frac{\partial}{\partial r}\left[r_\varepsilon \frac{\partial}{\partial r}\widehat{\widehat{\phi}}(r)\right] = {}_\varepsilon\widehat{\phi},$$

$$\frac{\partial}{\partial r}{}_\varepsilon\widehat{\widehat{\phi}} = \frac{1}{r}\int r_\varepsilon \widehat{\phi}(r)dr + \frac{c_3}{r}, \tag{15}$$

$${}_\varepsilon\widehat{\widehat{\phi}} = \int \frac{1}{r}\left[\int r_\varepsilon \widehat{\phi}(r)dr\right]\log(r) + c_4.$$

The selection of $c_1 = 1/2\pi$, $c_2 = 0$, $c_3 = 3\varepsilon^2/8\pi$, and $c_4 = 0$ gives the following harmonic and biharmonic rational blobs:

$${}_{\varepsilon\mathrm{rat}}\widehat{\phi} = \frac{1}{2\pi}\left\{\log\left[\left(r^2+\varepsilon^2\right)^{1/2}+\varepsilon\right] - \varepsilon\left(r^2+\varepsilon^2\right)^{-1/2}\right\}, \tag{16}$$

$${}_{\varepsilon\mathrm{rat}}\widehat{\widehat{\phi}} = \frac{1}{8\pi}\left\{\left(r^2+2\varepsilon^2\right)\log\left[\varepsilon+\left(r^2+\varepsilon^2\right)^{1/2}\right] - r^2 - \varepsilon\left(r^2+\varepsilon^2\right)^{1/2}\right\}. \tag{17}$$

The selection of $c_1 = 1/2\pi$, $c_2 = 0$, $c_3 = \varepsilon^2/8\pi$, and $c_4 = 0$ gives the following harmonic and biharmonic exponential blobs:

$${}_{\varepsilon\exp}\widehat{\phi} = -\frac{1}{4\pi}\mathrm{Ei}\left(-\frac{r^2}{\varepsilon^2}\right) + \frac{1}{2\pi}\log(r), \tag{18}$$

$${}_{\varepsilon\exp}\widehat{\widehat{\phi}} = -\frac{1}{16\pi}\left\{2r^2 + e^{-r^2/\varepsilon^2}\varepsilon^2 + \left(r^2+\varepsilon^2\right)\left[\mathrm{Ei}\left(-\frac{r^2}{\varepsilon^2}\right) - 2\log(r)\right]\right\}, \tag{19}$$

where Ei stands for the exponential integral function

$$\mathrm{Ei} = -\int_{-x}^{\infty}\frac{\exp(-t)}{t}dt. \tag{20}$$

The derivation of Eqs. (18) and (19) is detailed in [13]. The coefficients c_1, c_2, c_3, c_4 in the integration have been selected in such a way that the blobs are reduced to the fundamental solution of the Laplace equation and biharmonic equation for $\varepsilon \to 0$

$$\lim_{\varepsilon\to 0}{}_{\varepsilon\exp}\widehat{\phi} = \lim_{\varepsilon\to 0}{}_{\varepsilon\mathrm{rat}}\widehat{\phi} = \frac{1}{2\pi}\log(r), \tag{21}$$

$$\lim_{\varepsilon\to 0}{}_{\varepsilon\exp}\widehat{\widehat{\phi}} = \lim_{\varepsilon\to 0}{}_{\varepsilon\mathrm{rat}}\widehat{\widehat{\phi}} = \frac{1}{8\pi}r^2\left[\log(r)-1\right]. \tag{22}$$

The exponential and rational blobs for two desingularization parameters ε are shown in Fig. 1. The boundary of the domain is discretized with collocation points $\mathbf{p}_n$, $n = 1, 2, ..., N$, where the desingularized sources with $\mathbf{s}_n = \mathbf{p}_n$ and $\varepsilon = \varepsilon(\mathbf{s}_n)$ are placed. The unknown forces f_{xn} and f_{yn} in source points are determined from $2N \times 2N$ system of linear equations in such a way that the boundary conditions are satisfied. The system of equations has the following form:

$$\mathbf{Ax} = \mathbf{b}, \qquad A_{jn}x_n = b_j, \quad j = 1, 2, ..., 2N, \quad n = 1, 2, ..., 2N, \tag{23}$$

$$A_{(2j-1)(2n-1)} = \Upsilon_x^D(\mathbf{p}_j)\,c_{xxn}(\mathbf{p}_j) + \Upsilon_{xx}^N(\mathbf{p}_j)\,c_{xxn,x}(\mathbf{p}_j) + \Upsilon_{xy}^N(\mathbf{p}_j)\,c_{xxn,y}(\mathbf{p}_j), \tag{24}$$

$$A_{(2j-1)(2n)} = \Upsilon_x^D(\mathbf{p}_j)\,c_{xyn}(\mathbf{p}_j) + \Upsilon_{xx}^N(\mathbf{p}_j)\,c_{xyn,x}(\mathbf{p}_j) + \Upsilon_{xy}^N(\mathbf{p}_j)\,c_{xyn,y}(\mathbf{p}_j), \tag{25}$$

$$A_{(2j)(2n-1)} = \Upsilon_y^D(\mathbf{p}_j)\,c_{yxn}(\mathbf{p}_j) + \Upsilon_{yx}^N(\mathbf{p}_j)\,c_{yxn,x}(\mathbf{p}_j) + \Upsilon_{yy}^N(\mathbf{p}_j)\,c_{yxn,y}(\mathbf{p}_j), \tag{26}$$

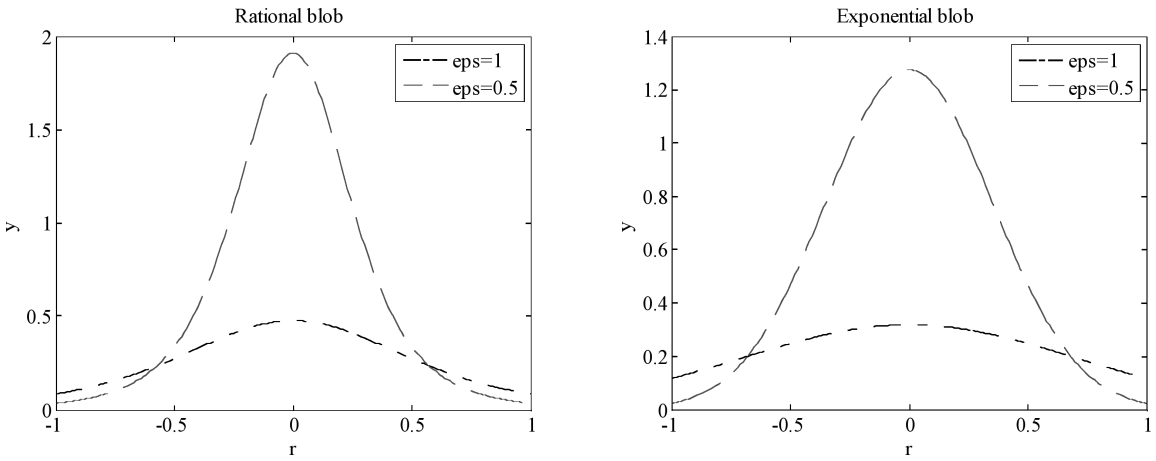

Fig. 1. Rational blob (left) and exponential blob (right).

$$A_{(2j)(2n)} = \Upsilon_y^D(\mathbf{p}_j)\, c_{yyn}(\mathbf{p}_j) + \Upsilon_{yx}^N(\mathbf{p}_j)\, c_{yyn,x}(\mathbf{p}_j) + \Upsilon_{yy}^N(\mathbf{p}_j)\, c_{yyn,y}(\mathbf{p}_j), \tag{27}$$

$$x_{2n-1} = f_{xn}, \tag{28}$$

$$x_{2n} = f_{yn}, \tag{29}$$

$$b_{2j-1} = \Upsilon_x^D(\mathbf{p}_j)\, \overline{v}_x(\mathbf{p}_j) + \Upsilon_{xx}^N(\mathbf{p}_j)\, \overline{v}_{xx}(\mathbf{p}_j) + \Upsilon_{xy}^N(\mathbf{p}_j)\, \overline{v}_{xy}(\mathbf{p}_j), \tag{30}$$

$$b_{2j} = \Upsilon_y^D(\mathbf{p}_j)\, \overline{v}_y(\mathbf{p}_j) + \Upsilon_{yx}^N(\mathbf{p}_j)\, \overline{v}_{yx}(\mathbf{p}_j) + \Upsilon_{yy}^N(\mathbf{p}_j)\, \overline{v}_{yy}(\mathbf{p}_j). \tag{31}$$

The following boundary conditions' indicators have been introduced in order to make the notation compact:

$$\Upsilon_\varsigma^D(\mathbf{p}) = \begin{cases} 1; & \mathbf{p} \in \Gamma_\varsigma^D \\ 0; & \mathbf{p} \notin \Gamma_\varsigma^D \end{cases}; \qquad \varsigma = x, y, \tag{32}$$

$$\Upsilon_{\varsigma\xi}^N(\mathbf{p}) = \begin{cases} 1; & \mathbf{p} \in \Gamma_{\varsigma\xi}^N \\ 0; & \mathbf{p} \notin \Gamma_{\varsigma\xi}^N \end{cases}; \qquad \varsigma, \xi = x, y, \tag{33}$$

as well as the following coefficients:

$$c_{xxn}(\mathbf{p}) = \frac{1}{\mu}\frac{\partial^2}{\partial p_x^2}{}_\varepsilon\widehat{\widehat{\phi}}(\mathbf{p} - \mathbf{s}_n) - \frac{1}{\mu}{}_\varepsilon\widehat{\phi}(\mathbf{p} - \mathbf{s}_n), \tag{34}$$

$$c_{xyn}(\mathbf{p}) = \frac{1}{\mu}\frac{\partial^2}{\partial p_x p_y}{}_\varepsilon\widehat{\widehat{\phi}}(\mathbf{p} - \mathbf{s}_n), \tag{35}$$

$$c_{yxn}(\mathbf{p}) = \frac{1}{\mu}\frac{\partial^2}{\partial p_x p_y}{}_\varepsilon\widehat{\widehat{\phi}}(\mathbf{p} - \mathbf{s}_n), \tag{36}$$

$$c_{yyn}(\mathbf{p}) = \frac{1}{\mu}\frac{\partial^2}{\partial p_y^2}{}_{\varepsilon}\widehat{\widehat{\phi}}(\mathbf{p}-\mathbf{s}_n) - \frac{1}{\mu}{}_{\varepsilon}\widehat{\phi}(\mathbf{p}-\mathbf{s}_n), \tag{37}$$

$$c_{\varsigma\xi n,\zeta} = \frac{\partial}{\partial p_\zeta} c_{\varsigma\xi n}, \qquad \varsigma,\xi,\zeta = x,y, \tag{38}$$

$$c_{xn}(\mathbf{p}) = \frac{\partial}{\partial p_x}{}_{\varepsilon}\widehat{\phi}(\mathbf{p}-\mathbf{s}_n), \tag{39}$$

$$c_{xn}(\mathbf{p}) = \frac{\partial}{\partial p_x}{}_{\varepsilon}\widehat{\phi}(\mathbf{p}-\mathbf{s}_n). \tag{40}$$

After calculating the forces from the system (23), the velocity components and pressure can be determined as

$$v_x(p_x,p_y) = \sum_{n=1}^{N}\left[c_{xxn}(p_x,p_y) f_{xn} + c_{xyn}(p_x,p_y) f_{yn}\right], \tag{41}$$

$$v_y(p_x,p_y) = \sum_{n=1}^{N}\left[c_{yxn}(p_x,p_y) f_{xn} + c_{yyn}(p_x,p_y) f_{yn}\right], \tag{42}$$

$$P(p_x,p_y) = \sum_{n=1}^{N}\left[c_{xn}(p_x,p_y) f_{xn} + c_{yn}(p_x,p_y) f_{yn}\right]. \tag{43}$$

4. Numerical examples

Example 1. Let us consider a rectangular cavity with dimensions $p_{x-} \le p_x \le p_{x+}$, $p_{y-} \le p_y \le p_{y+}$, $p_{x-} = p_{y-} = -0.5$ m with $p_{x+} = p_{y+} = +0.5$ m. The boundary conditions are of the Dirichlet type on all the four boundaries. The velocity is set to 0 m/s at the south, east and west boundaries, and to $v_x = 1$ m/s, $v_y = 0$ m/s, at the north boundary. This setting represents the standard driven cavity problem [14] with Stokes flow instead of the Navier-Stokes flow. The reference solution to the problem is obtained by the classical second- order FDM on uniform 91×91 and 101×101 node arrangements. Both solutions are interpolated by the cubic splines to 501×501 uniform node arrangement. The root mean square (RMS) error between the solutions is then calculated by

$$L_2 = \sqrt{\frac{1}{501\times 501}\left\{\left[\mathrm{I}_{101}^{501}(v_{xi,j}) - \mathrm{I}_{91}^{501}(v_{xi,j})\right]^2 + \left[\mathrm{I}_{101}^{501}(v_{yi,j}) - \mathrm{I}_{91}^{501}(v_{yi,j})\right]^2\right\}}, \tag{44}$$

where the function $\mathrm{I}_{N_1}^{N_2}[\theta(\mathbf{p})]$ represents the cubic spline interpolation of the scalar function $\theta(\mathbf{p})$ from the regular node arrangement $N_1 \times N_1$ to the regular node arrangement $N_2 \times N_2$. The RMS error between the two obtained solutions is $L_2 = 6.22 \times 10^{-4}$ and the maximum error is $L_\infty = 5.02 \times 10^{-2}$ which confirms a reasonable mesh independence of the 101×101 solution that is used in all subsequent comparisons. The discretization of the present method and the FDM is shown in Fig. 2.

Figure 3 represents the sensibility of the solution as a function of the desingularization parameter. A comparison of the fine-grid 101×101 FDM solution with the MRS solutions, based on rational and exponential blobs, is given in Figs. 5 and 6, respectively. Convergence of the method with finer boundary discretization is demonstrated. The variation of error in L_2 norm with ε is assessed. We found out that reliable results can be obtained in the cases $0.1\Delta_\varsigma \le \varepsilon \le 0.3\Delta_\varsigma$, where Δp_ς stands for the nodal distance. The behavior of the solutions obtained by the rational and exponential blobs is very similar.

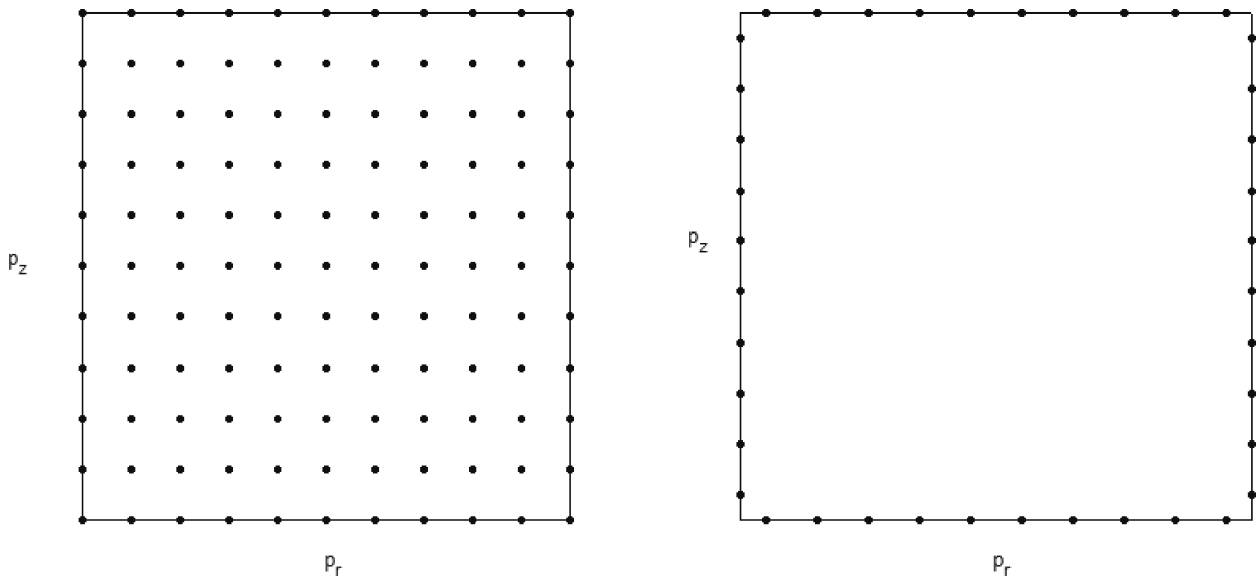

Fig. 2. Discretization schematics of the driven cavity problem. FDM (left) and MRS (right).

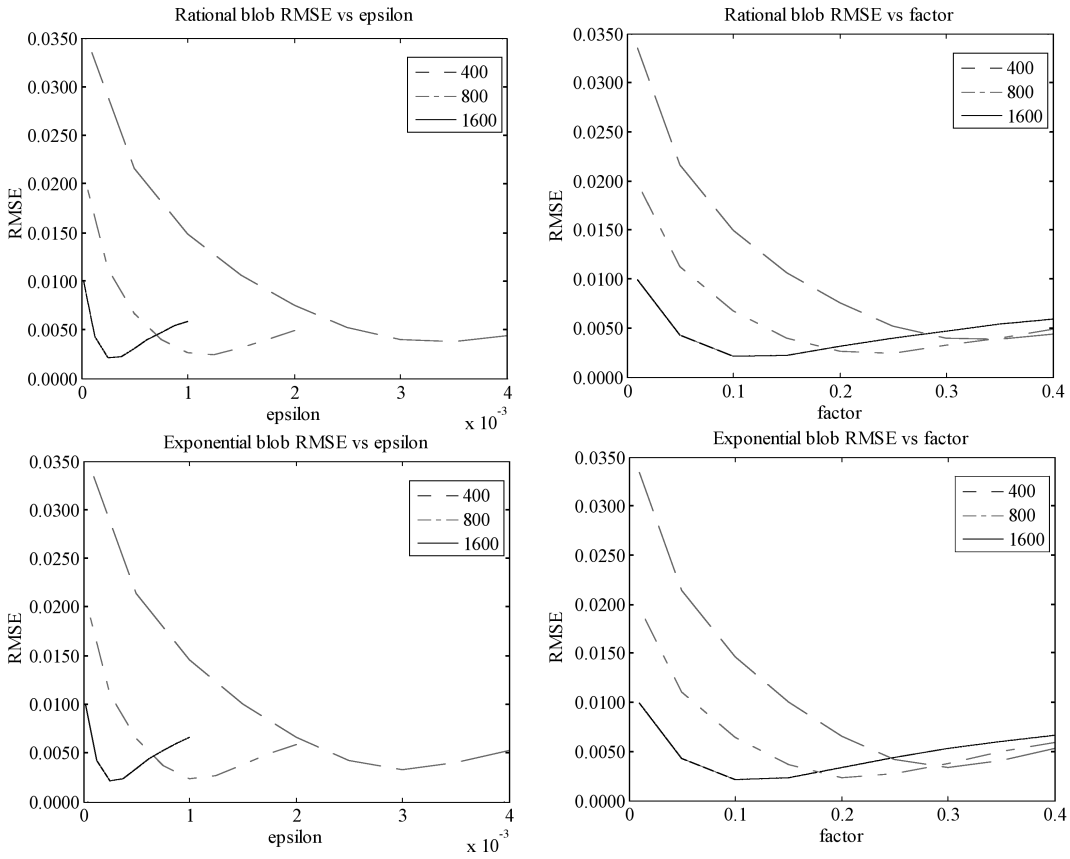

Fig. 3. L_2 error of the MRS solution by using rational (top) and exponential (bottom) blobs versus 101×101 FDM solution as a function of ε (left) and as a function of the factor f_ε (right) between epsilon and nodal distance ($f_\varepsilon = \varepsilon/\Delta p_\varsigma$). The RMS error between the solutions is calculated on a uniform 501×501 node arrangement.

Example 2. Let us consider a flow between two parallel plates with the dimensions $p_{x-} \le p_x \le p_{x+}$, $p_{y-} \le p_y \le p_{y+}$, $p_{x-} = -5.0m$, $p_{y-} = -0.5$ m with $p_{x+} = +5.0$ m, $p_{y+} = +0.5$ m. The boundary

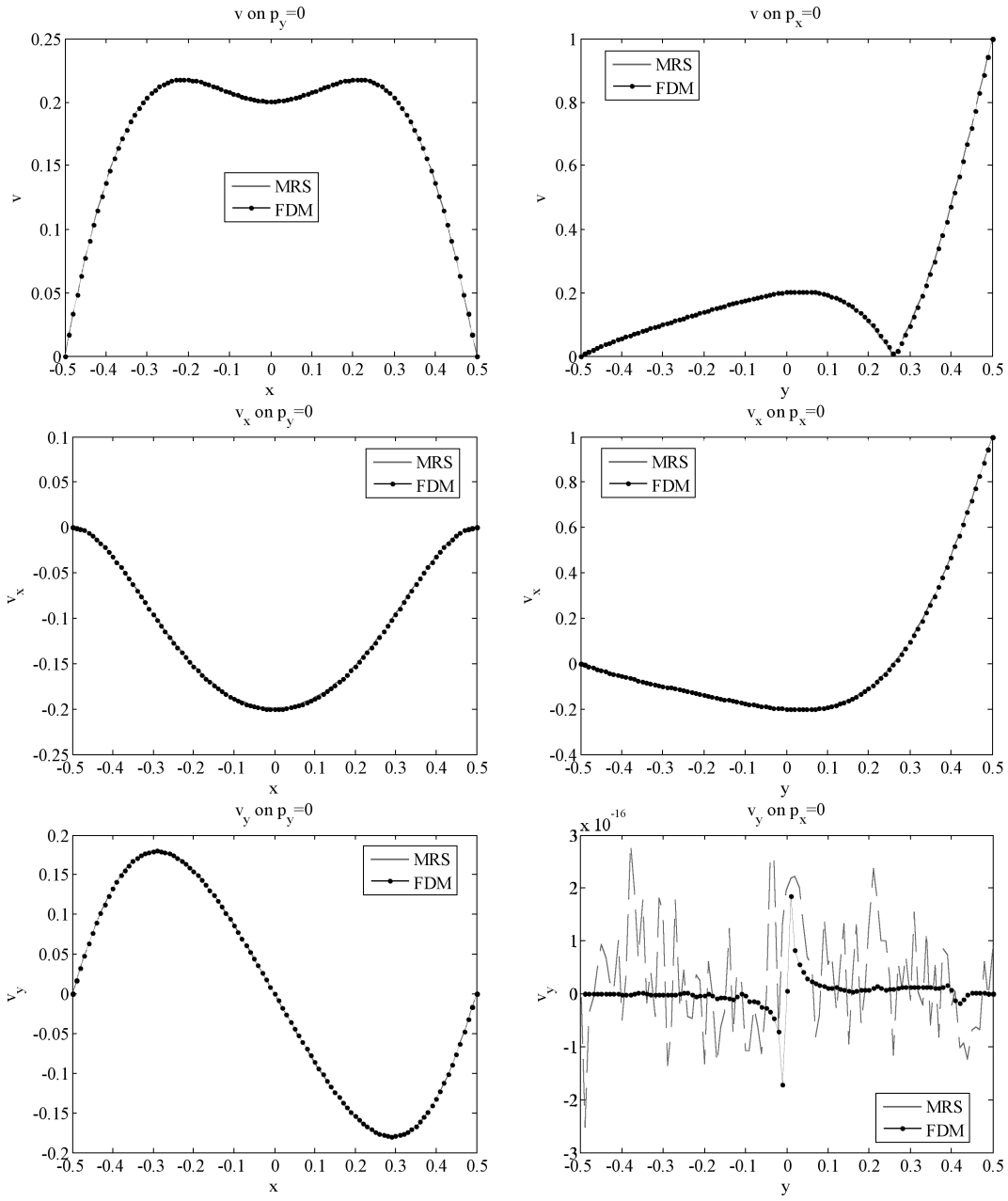

Fig. 4. Comparison between MRS solutions, by using rational blobs with a uniform node arrangement $N = 800$, $\varepsilon = 0.001$, and 101×101 FDM solution.

conditions are of the Dirichlet type on the four boundaries. The velocity is set to $v_x = v_y = 0$ m/s at the south and north boundaries, and to $v_x = -\dfrac{\Delta P}{2\mu}(y - y_-)(y_+ - y)$ m/s, $v_y = 0$ m/s, at the west and east boundaries. The boundary conditions define a developed flow in the pipe with fluid viscosity μ and pressure drop $\Delta P = -1$ N/m^2, set to $\mu = 1$ kg/(ms) and $\Delta P = -1$ N/m^2. The numerical solution is calculated for 2200 uniform nodes on the boundary (1000 on the north and south boundaries, and 100 on the west and east boundaries). The root mean square (RMS) error L_2 between the solutions is calculated as a function of the shape parameter. The results are given in Fig. 6. The analytical solution of the velocity derivative is $\dfrac{\partial}{\partial p_y} v_x = \dfrac{\Delta P}{\mu} y$ m/s, and the velocity derivative is evaluated at 101 points across the line $p_{y-} \leq p_y \leq p_{y+}$ at $p_x = (p_{x+} + p_{x-})/2$. All the

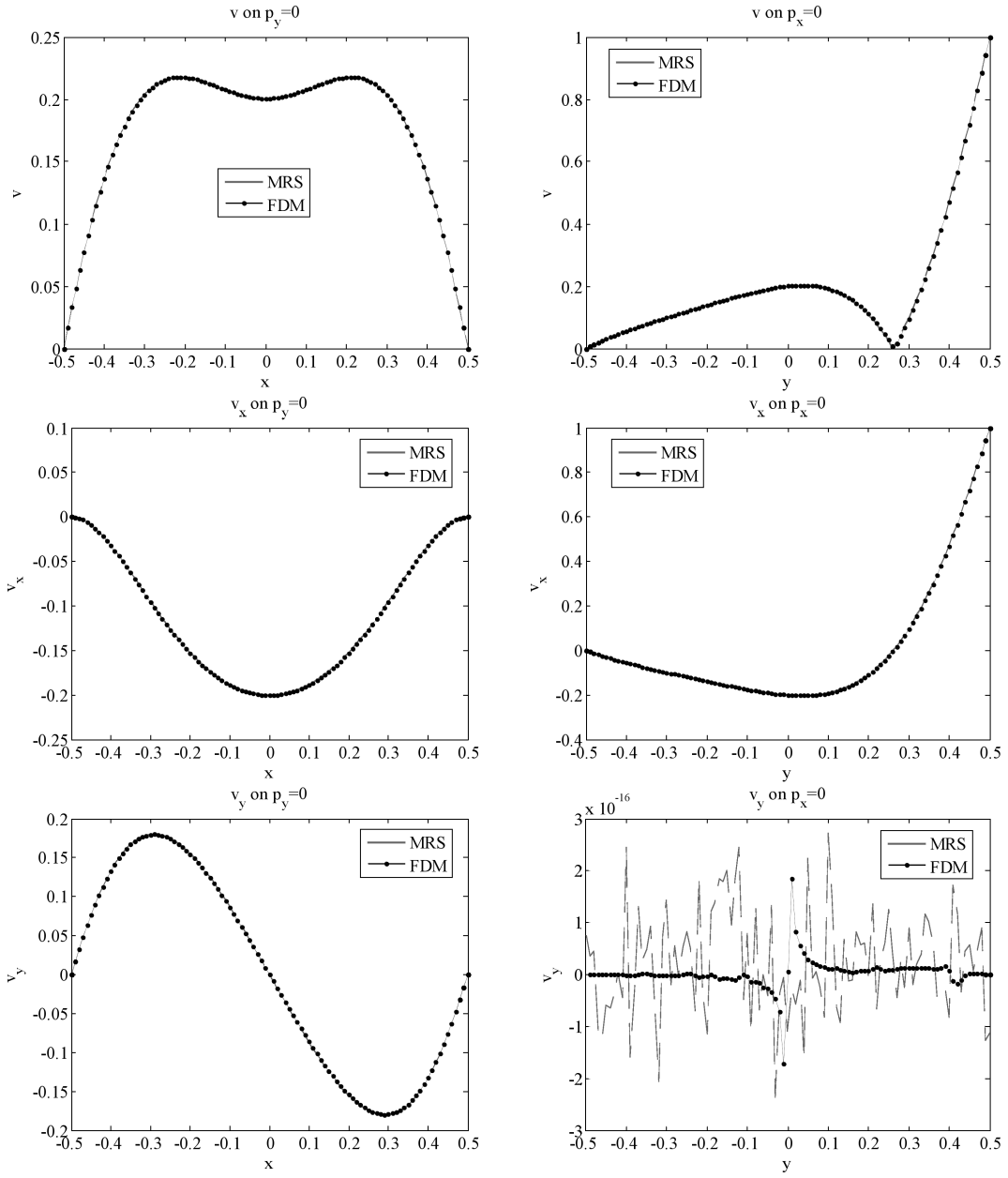

Fig. 5. Comparison between MRS solutions, by using exponential blobs with a uniform node arrangement $N = 800$, $\varepsilon = 0.001$, and 101×101 FDM solution.

figures below are arranged so that the upper figures represent rational blobs and the lower figures represent exponential blobs.

Comparison of computing times of Intel Fortran code run on a modern PC by using rational and exponential blobs gives the following results. Example 1 with 800 nodes and $f_\varepsilon = 0.1$ takes 0.83 s of computing time with rational blob and 1.15 s of computing time with exponential blob, respectively. Example 2 with 2200 nodes and $f_\varepsilon = 0.6$ takes 7.40 s of computing time with rational blob and 9.63 s of computing time with exponential blob, respectively. The related rational blob solution in Example 1 has the RMS error of 2.55e-03, and in Example 2 the RMS error is 8.35-06. The related exponential blob solution, in Example 1, has the RMS error of 2.31e-03, and in Example 2 the RMS error is 4.24e-06. From the given numbers, one can see that the exponential blob gives slightly more accurate results for a slightly higher computational cost.

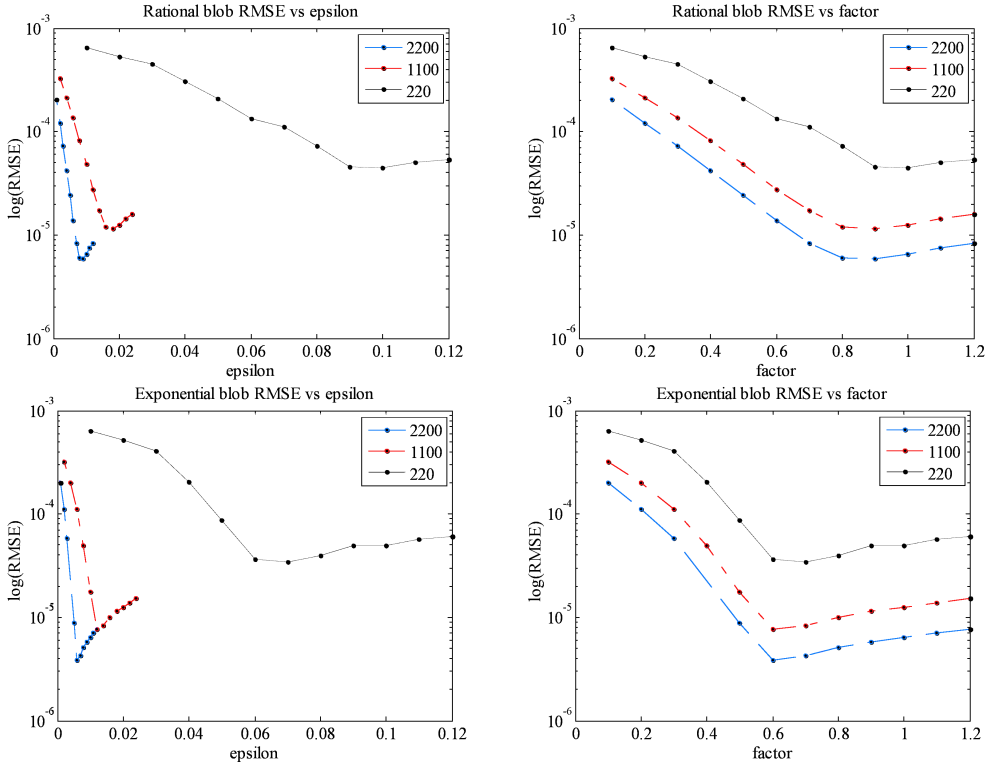

Fig. 6. L_2 error of MRS solution with rational (top) and exponential (bottom) blobs of v_x as a function of ε (left) and as a function of the factor f_ε (right) between epsilon and nodal distance ($f_\varepsilon = \varepsilon/\Delta p_\varsigma$). The RMS error between the solutions is calculated on a uniform 101 node arrangement across the line $p_{y-} \le p_y \le p_{y+}$ at $p_x = (p_{x+} + p_{x-})/2$.

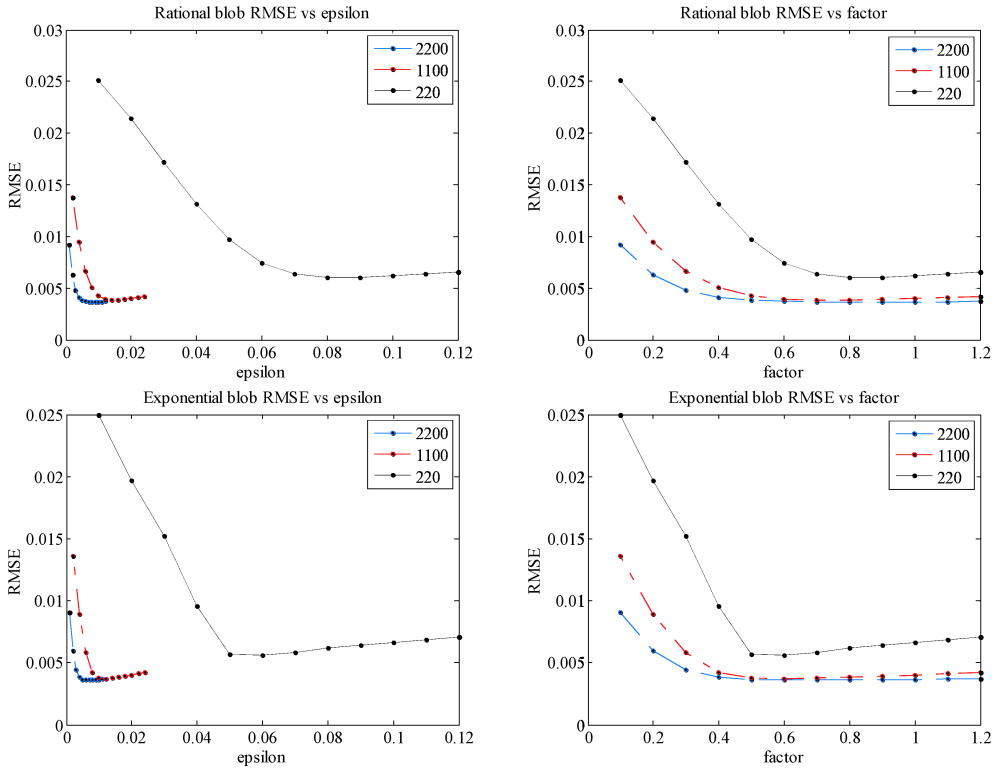

Fig. 7. L_2 error of the MRS solution with rational and exponential blobs of $\partial v_x/\partial p_y$ as a function of ε (left) and as a function of the factor f_ε (right) between epsilon and nodal distance ($f_\varepsilon = \varepsilon/\Delta p_\varsigma$). The RMS error between the solutions is calculated on a uniform 101 node arrangement across the line $p_{y-} \le p_y \le p_{y+}$ at $p_x = (p_{x+} + p_{x-})/2$.

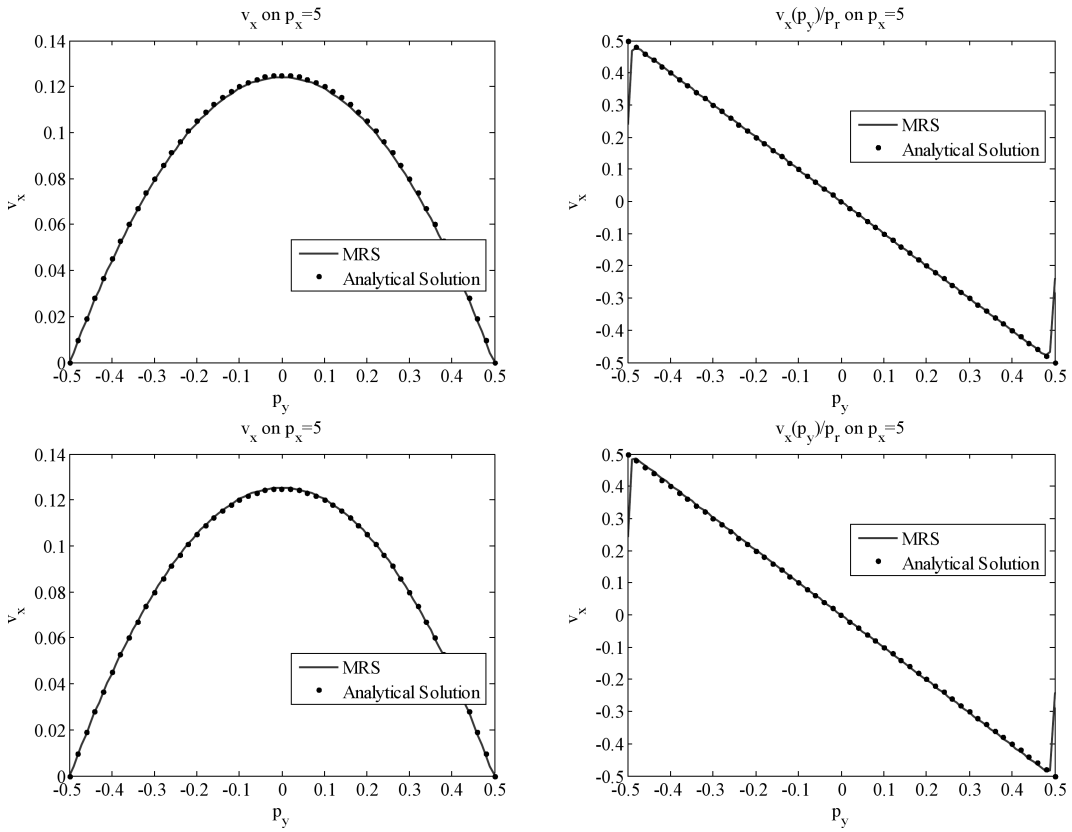

Fig. 8. Profile of v_x (left) and $\partial v_x/\partial p_y$ (right) calculated by MRS with rational (upper) and exponential (lower) blobs and analytical solution, evaluated at $N = 101$, $\varepsilon = 0.007$ across the line $p_{y-} \leq p_y \leq p_{y+}$ at $p_x = (p_{x+} + p_{x-})/2$.

5. Conclusions

The presented, in this paper, novel MRS is a very simple and efficient boundary meshless method without artificial boundary. The solution is constructed through the superposition of the exact solutions due to regularized sources placed on the physical boundary of the system. The coefficients of the trial functions, obtained in this way, are requiring the solution to comply with the boundary conditions. The method has been assessed for the first time for the problem involving the driven cavity and the flow between parallel plates. A study of the performance of the method when using different types of blobs: rational and exponential, has been performed. Accurate results can be obtained when the regularization parameter scales with the typical nodal distance. In the future, this method can be connected with a robust algorithm for an estimation of the specific optimum regularization parameter for each of the boundary nodes separately. If needed, this would make possible to obtain even more accurate results. Such an algorithm might be of the leave-one-out-cross-validation-type [15], as recently demonstrated for the determination of artificial boundary position in classic MFS. A development of the axisymmetric version of the formulation that would cope with free and moving boundary problems such as the ones appearing between gas and liquid (gas focusing micro-jets) is published in [12].

Acknowledgements

The present paper is sponsored by Slovenian Grant Agency under program group P2-0379, bilateral project China-Slovenia (2014–2015), and the project: Innovative methods for imaging with the X-ray free-electron laser (XFEL) and synchrotron sources, sponsored by Desy, Germany.

The project is also supported by the National Natural Science Foundation of China (Grant No. 11472184) and the National Youth Science Foundation of China (Grant No. 11401423).

References

[1] D.J. Acheson. *Elementary Fluid Dynamics*. Oxford Applied Mathematics and Computing Science Series, Oxford, England, 1990.

[2] K.R. Beyerlein, L. Adriano, M. Heymann, R. Kirian, J. Knoška, F. Wilde, H.N. Chapman, S. Bajt. Ceramic micro-injection molded nozzles for serial femtosecond crystallography sample delivery. *Review of Scientific Instruments*, **86**: 125104, 2015, http://dx.doi.org/10.1063/1.4936843.

[3] W. Chen, Z.J. Fu, C.S. Chen. *Recent Advances in Radial Basis Function Collocation Methods*. Springer Briefs in Applied Sciences and Technology, Springer, Heidelberg, 2014.

[4] D.L. Young, K.H. Chen, C.W. Lee. Novel meshless method for solving the potential problems with arbitrary domain. *Journal of Computational Physics*, **209**: 290–322, 2006.

[5] D.L. Young, S.J. Jane, C.M. Fan, K. Murgesan, C.C. Tsai. The method of fundamental solutions for 2D and 3D Stokes problems. *Journal of Computational Physics*, **211**: 1–8, 2006.

[6] A.E. Curteanu, L. Elliot, D.B. Ingham, D. Lesnic. Laplacian decomposition and the boundary element method for solving Stokes problems. *Engineering Analysis with Boundary Elements*, **31**: 501–513, 2007.

[7] B. Šarler. Solution of potential flow problems by the modified method of fundamental solutions: formulations with the single layer and the double layer fundamental solutions. *Engineering Analysis with Boundary Elements*, **33**: 1374–1382, 2009.

[8] M. Perne, B. Šarler, F. Gabrovšek. Calculating transport of water from a conduit to the porous matrix by boundary distributed source method. *Engineering Analysis with Boundary Elements*, **36**: 1649–1659, 2012.

[9] E. Sincich, B. Šarler. Non-singular method of fundamental solutions based on Laplace decomposition for 2D Stokes flow problems. *Computer Modeling in Engineering & Sciences*, **99**: 393–415, 2014.

[10] R. Cortez. The method of regularized Stokeslets. *SIAM Journal of Scientific Computing*, **23**: 1204–1225, 2005.

[11] R. Cortez, L. Fauci, A. Medovikov. The method of regularized Stokeslets in three dimensions: analysis, validation, and application to helical swimming. *Physics of Fluids*, **17**: 031504–1, 031504–14, 2005.

[12] K. Wang, S.T. Wen, R. Zahoor, M. Li, B. Šarler. Method of regularized sources for axisymmetric Stokes flow problems. *International Journal of Numerical Methods for Heat & Fluid Flow*, **26**(3/4): 1226–1239, 2016.

[13] A.R. Lamichhane, C.S. Chen. The closed-form particular solutions for Laplace and biharmonic operators using Gaussian radial basis function. *Applied Mathematics Letters*, **46**: 50–56, 2015.

[14] U. Ghia, K.T. Ghia, C.T. Shin. High-Re solutions for incompressible flow using the Navier-Stokes equations and a multigrid method. *Journal of Computational Physics*, **48**, 387–411, 1982.

[15] C.S. Chen, A. Karageorghis, Y. Li. *On choosing the location of the sources in MFS*. Numerical Algorithms, DOI: 10.1007/s11075-015-0036-0, 2016.